



## Fracture morphology and its evolution A review on crack path stability and brittle fracture along butt-weld

Y. Sumi

Yokohama National University, Japan

sumi@ynu.ac.jp

**ABSTRACT.** Considerations are made for the fracture morphology and its evolution in relation to the brittle fracture along butt-weld, where crack path stability may play important roles in various aspects. Analyses of a kinked and curved crack are first reviewed in the present paper. Having learned the solutions of a kinked and curved crack, several crack path criteria are compared for the crack path prediction. Then, some aspects of stability of a crack path are examined as to whether it may propagate, keeping its original direction or not in a homogeneous material, and whether crack kinking in a material having inhomogeneous fracture toughness may be predicted by seeking the state which gives rise to an energetically stable one. Having reviewed the morphology of brittle crack propagation along butt-weld, brittle fracture of extremely thick plates of high tensile steel is discussed for the fracture control of recently emerging large container ships.

**KEYWORDS.** Curved crack; Kinked crack; Crack path criteria; Crack path stability; Butt-weld; Extremely thick plate.

### INTRODUCTION

Analyses of a kinked and curved crack are reviewed in the present paper focusing attention on the brittle crack propagation along butt-weld. The perturbation solutions of a slightly curved crack [1-8] are compared with analytical solutions [9, 10]. Having learned the solutions of a kinked and curved crack, several crack path criteria are compared for the crack path prediction, where criteria may be derived from a stress state prior to the crack propagation [11], the geometrical continuity condition of crack surfaces [1-3], or an energetically favorable condition after crack growth [9]. Then, some aspects of stability of a crack path are examined as to whether it may propagate, keeping its original direction or not in a homogeneous material [12], and whether crack kinking in a material having inhomogeneous fracture toughness may be predicted by energetic stability [7].

Crack path stability in a symmetric homogeneous brittle solid is reviewed [13-15], where the geometry of the body is symmetric with respect to the initial straight-crack line, and where the presence of a small asymmetric loading or slight material inhomogeneity which may produce a small Mode-II stress-intensity factor  $k_{II}$  at the original crack tip, leads to non-collinear crack growth. The crack path stability is then examined by taking into account the curved trajectory predicted by the local symmetry criterion [12].

Lastly, having reviewed experimental and theoretical studies of brittle crack propagation paths along butt-weld [7, 16], the concept of fracture control applied to extremely thick plates of high tensile steel is discussed for the structural design of large container ships [17].

## SOLUTIONS OF A CURVED CRACK

The problem of a slightly non-collinear, quasi-static crack growth is considered. Problems of this kind have been treated by a first order perturbation method, in the context of Muskhelishvili's complex potentials [18], by Banichuk [1] and Goldstein and Salganik [2,3]. Cotterell and Rice [4] employed the same method and obtained a rather simple first order expression for the stress intensity factors, which were used to examine the crack growth path of a semi-infinite crack in an infinitely extended domain. We shall consider the first and second order perturbation solutions which can take into account the effects of the geometry of the domain, i.e., finite outer boundaries as well as the finite crack length, Sumi *et al.* [5], Sumi [6,7]. For this purpose we first calculate the perturbation solution for a semi-infinite straight crack with a slightly kinked and curved extension, which will be used as the fundamental solution of the problem. We can establish the effect of the geometry of the domain by considering the far field behavior of the fundamental solution.

### Second Order Perturbation Solution

Consider a homogeneous linearly elastic brittle solid containing a straight crack of length  $a$ . The stress tensor and the displacement vector  $\sigma_{ij}$  and  $u_i$  are defined in the domain  $V$  occupied by the body. Surface tractions,  $t_i$ , are prescribed on the part of the outer boundary,  $S_t$ , and on the crack faces,  $S_c^\pm$ , while surface displacements,  $v_i$ , are prescribed on the remaining part of the outer boundary,  $S_u$  (see Fig. 1). The Cartesian coordinate system  $(x_1, x_2)$  with the origin at the crack tip has its  $x_1$ -axis along with the original crack line. In the following analysis this problem is referred to as the original problem.

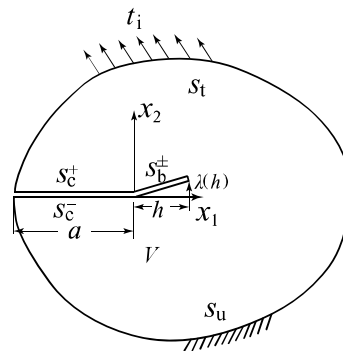


Figure 1: Straight crack with slightly kinked and curved extension.

For a slightly non-symmetric loading system, we may have a slightly kinked and curved crack extension, whose projected length on the  $x_1$ -axis is  $h$ , and whose deviation from the  $x_1$ -axis is  $\lambda(h)$ . To investigate the detailed distribution of stresses ahead of the extended crack tip, we consider the second order perturbation solution of the semi-infinite straight crack with slightly kinked and curved extension, whose near tip field solution gives the stress intensity factors. Then we account for the effect of the finite outer boundary by using the far field solution of the semi-infinite crack. In the following analysis we assume that the shape of the crack extension can be approximated by

$$\lambda(x_1) = \alpha x_1 + \beta x_1^{3/2} + \gamma x_1^2, \quad (1)$$

disregarding higher order terms. Constants  $\alpha$ ,  $\beta$ , and  $\gamma$  are considered as shape parameters of the crack extension. This expression has the appropriate asymptotic form associated with the stress field ahead of a preexisting crack tip. The crack profile may be determined based on an appropriate crack path criterion which will be discussed in the following section. As is shown in Fig. 2, another linear orthogonal coordinate system  $(\xi_1, \xi_2)$  is introduced,

$$\xi_1 = x_1, \quad (2)$$

and the crack path deviation from the  $\xi_1$ -axis is measured by



$$\eta(\xi_1) = \lambda(\xi_1) - \lambda(b), \tag{3}$$

Following the same method as used by Banichuk [1], Goldstein and Salganik [2, 3], and Cotterell and Rice [4], the perturbation solution of the stress field can be expressed by Muskhelishvili's analytic functions [18] given by

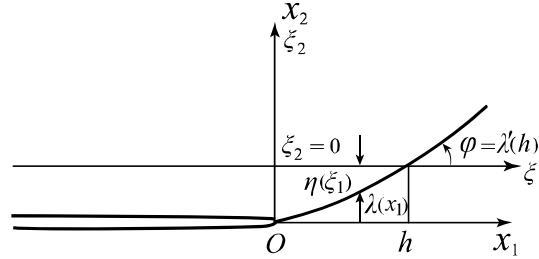


Figure 2: Coordinate systems for a kinked and curved crack.

$$\begin{aligned} \sigma_{11} + \sigma_{22} &= 2[\psi'(z) + \overline{\psi'(z)}], \\ \sigma_{22} - \sigma_{11} - 2i\sigma_{12} &= 2[(z - \bar{z})\psi''(z) + \omega(z) - \overline{\psi'(z)}], \end{aligned} \tag{4}$$

where  $z = x_1 + ix_2$ . The analytic functions  $\psi(z)$  and  $\omega(z)$  are expanded in terms of  $\eta(\xi_1)$  up to the second order in the following form:

$$\begin{aligned} \psi'(z) &= \psi'_0(z) + \psi'_1(z) + \psi'_2(z) + O(\eta^3), \\ \omega(z) &= \omega_0(z) + \omega_1(z) + \omega_2(z) + O(\eta^3), \end{aligned} \tag{5}$$

in which  $\psi_0(z)$  and  $\omega_0(z)$  are of the zero-th order,  $\psi_1(z)$  and  $\omega_1(z)$  are of the first order, and  $\psi_2(z)$  and  $\omega_2(z)$  are of the second order in  $\eta(\xi_1)$ . The boundary conditions on the crack surfaces, at  $z = \xi_1 + i\eta(\xi_1)$  become

$$\psi'(Z) + \overline{\psi'(z)} + e^{-2i\varphi}[(z - \bar{z})\psi''(z) + \omega(z) - \overline{\psi'(z)}] = -(T_n - iT_s), \tag{6}$$

where  $\varphi$  is the angle of the slope on the crack line. It is assumed that the crack surfaces are subjected to normal and shear tractions  $T_n$  and  $T_s$  on the upper surface and  $-T_n$  and  $-T_s$  on the lower surface, respectively. We also assume that tractions on the crack surfaces,  $T_n$  and  $T_s$  are bounded and integrable in the defined range.

*Approximate Description of a Slightly Kinked and Curved Extension of a Straight Crack*

The second order approximation of the stress distribution in the vicinity of the original crack tip can be expressed by

$$\sigma_{ij} = \sigma_{ij}(x_1, 0) + \sigma_{ij,2}(x_1, 0)\lambda + \frac{1}{2}\sigma_{ij,22}(x_1, 0)\lambda^2 + O(\lambda^3), \tag{7}$$

in which

$$\begin{aligned} \sigma_{11}(x_1, 0) &= \frac{k_I}{\sqrt{2\pi x_1}} + T + b_I \sqrt{\frac{x_1}{2\pi}} + O(x_1), \\ \sigma_{22}(x_1, 0) &= \frac{k_I}{\sqrt{2\pi x_1}} + b_I \sqrt{\frac{x_1}{2\pi}} + O(x_1), \\ \sigma_{12}(x_1, 0) &= \frac{k_{II}}{\sqrt{2\pi x_1}} + b_{II} \sqrt{\frac{x_1}{2\pi}} + O(x_1), \end{aligned} \tag{8}$$

where  $k_I$  and  $k_{II}$  are the stress intensity factors, and the coefficients  $T$ ,  $b_I$ , and  $b_{II}$  are also determined from the solution of the boundary-value problem prior to the crack extension. The surface tractions on the extended crack surfaces,  $T_n$  and  $T_s$



can be calculated by using Eq.(7), and the stress intensity factors at the extended crack tip in an infinite plane can be obtained as

$$K_I^{(\infty)} = \left(1 - \frac{3}{8}\alpha^2\right)k_1 - \frac{3}{2}\alpha k_{II} - \left(\frac{9}{4}\beta k_{II} + \frac{9}{8}\alpha\beta k_1 - 2\sqrt{\frac{2}{\pi}}\alpha^2 T\right)b^{1/2} + \left[\frac{1}{2}\left(1 + \frac{9}{8}\alpha^2\right)b_1 - 3\gamma k_{II} - \frac{5}{4}\alpha b_{II}\right. \\ \left. + \frac{11}{2}\sqrt{\frac{2}{\pi}}\alpha\beta T - \left(\frac{27}{32}\beta^2 + \frac{3}{2}\alpha\gamma\right)k_1\right]b + O(b^{3/2}), \quad (9)$$

$$K_{II}^{(\infty)} = \left(1 - \frac{7}{8}\alpha^2\right)k_{II} + \frac{1}{2}\alpha k_1 + \left\{\frac{3}{4}\beta k_1 - 2\sqrt{\frac{2}{\pi}}\alpha T + \left(-\frac{21}{8} + \frac{2}{\pi}\right)\alpha\beta k_{II}\right\}b^{1/2} + \left[\frac{1}{2}\left(1 - \frac{27}{8}\alpha^2\right)b_{II} + \gamma k_1\right. \\ \left. - \frac{\alpha}{4}b_1 - \frac{3}{4}\sqrt{2\pi}\beta T - \left\{\left(\frac{63}{32} - \frac{2}{\pi}\right)\beta^2 + \frac{5}{2}\alpha\gamma\right\}k_{II}\right]b + O(b^{3/2}). \quad (10)$$

As far as the terms obtained by Wu [9], and Amestoy and Leblond [10] are concerned, Eq. (9) represents the exact second order asymptotic behavior of the Mode-I stress intensity factor, while the second order terms in Eq. (10) are approximate. Although being small, this slight numerical difference may arise from the interaction of stress singularities between the kinked corner and the crack tip.

#### *Stress Intensity Factors for a Finite Body*

Since the leading terms of the far-field stress and displacement are of the order of the crack extension length  $h$  [7], the finite body corrections of the stress intensity factors at the kinked and curved crack tip are given by

$$K_I^{(f)} = \left[\left\{\left(1 - \frac{3}{8}\alpha^2\right)k_1 - \alpha k_{II}\right\}\overline{k_{11}} + \left\{\left(1 - \frac{1}{8}\alpha^2\right)k_{II} - \alpha k_1\right\}\overline{k_{12}}\right. \\ \left. - \frac{3}{2}\alpha(k_1 - \alpha k_{II})\overline{k_{21}} - \frac{3}{2}\alpha(k_{II} - \alpha k_1)\overline{k_{22}}\right]b + O(b^{3/2}), \quad (11)$$

$$K_{II}^{(f)} = \left[\left\{\left(1 - \frac{7}{8}\alpha^2\right)k_1 - \alpha k_{II}\right\}\overline{k_{21}} + \left\{\left(1 - \frac{5}{8}\alpha^2\right)k_{II} - \alpha k_1\right\}\overline{k_{22}}\right. \\ \left. + \frac{1}{2}\alpha(k_1 - \alpha k_{II})\overline{k_{11}} + \frac{1}{2}\alpha(k_{II} - \alpha k_1)\overline{k_{12}}\right]b + O(b^{3/2}), \quad (12)$$

where  $\overline{k_{11}}$ ,  $\overline{k_{21}}$  and  $\overline{k_{12}}$ ,  $\overline{k_{22}}$  correspond to the stress intensity factors of Mode-I and Mode-II for the Mode-I and Mode-II fundamental fields [19], respectively, [5, 6,7]. The stress intensity factors  $K_I$  and  $K_{II}$ , at the kinked and curved crack tip are accordingly obtained by the sum of Eqs. (9) and (11), and the sum of Eqs. (10) and (12) given by,

$$K_I = K_I^{(\infty)} + K_I^{(f)} + O(b^{3/2}), \quad (13)$$

$$K_{II} = K_{II}^{(\infty)} + K_{II}^{(f)} + O(b^{3/2}). \quad (14)$$

If we only retain the first order terms with respect to  $\eta(\xi_1)$ , the solution is simplified as

$$K_I = \left(k_1 - \frac{3}{2}\alpha k_{II}\right) - \frac{9}{4}\beta k_{II}b^{1/2} + \left[\frac{b_1}{2} - \frac{5}{4}\alpha b_{II} - 3\gamma k_{II} + k_1\overline{k_{11}}\right. \\ \left. - \alpha k_1\left(\overline{k_{12}} + \frac{3}{2}\overline{k_{21}}\right) + k_{II}\overline{k_{12}} - \alpha k_{II}\left(\overline{k_{11}} + \frac{3}{2}\overline{k_{22}}\right)\right]b + O(b^{3/2}), \quad (15)$$



$$\begin{aligned}
 K_{II} = & \left( k_{II} + \frac{\alpha}{2} k_I \right) + \left( \frac{3}{4} \beta k_I - 2 \sqrt{\frac{2}{\pi}} \alpha T \right) b^{1/2} + \left[ \frac{b_{II}}{2} - \frac{\alpha}{4} b_I - \frac{3}{4} \sqrt{2\pi} \beta T + \gamma k_I + k_I \overline{k_{21}} \right. \\
 & \left. + \alpha k_I \left( \frac{1}{2} \overline{k_{11}} - \overline{k_{22}} \right) + k_{II} \overline{k_{22}} + \alpha k_{II} \left( \frac{1}{2} \overline{k_{12}} - \overline{k_{21}} \right) \right] b + O(b^{3/2}).
 \end{aligned}
 \tag{16}$$

### CRACK PATH CRITERIA

Having obtained the stress intensity factors of a slightly kinked and curved crack, investigations are made for possible crack paths along which fracture takes place. Several aspects should be taken into account, such as the stress state prior to crack extension, geometrical continuity of a crack path, and the change of energy along different crack paths. The stress field ahead of a crack tip has been obtained for Mode-I and Mode-II, respectively, and the corresponding hoop stress component of is expressed by

$$\sigma_{\theta} = \frac{k_I}{\sqrt{2\pi r}} \left( \frac{3}{4} \cos \frac{\theta}{2} + \frac{1}{4} \cos \frac{3\theta}{2} \right) - \frac{k_{II}}{\sqrt{2\pi r}} \left( \frac{3}{4} \sin \frac{\theta}{2} + \frac{3}{4} \sin \frac{3\theta}{2} \right).
 \tag{17}$$

The solution of a straight kink of a finite kink angle was obtained by Bilby and Cardew [20], Bilby *et al.* [21], Hayashi and Nemat-Nasser [22], Leblond [23], and Amestoy and Leblond [10], where the analytical expression of the stress intensity factors ahead of the kinked tip was obtained by Amestoy and Leblond [10] in the following form:

$$K_I(\alpha) = F_{11}(\alpha) k_I + F_{12}(\alpha) k_{II},
 \tag{18}$$

$$K_{II}(\alpha) = F_{21}(\alpha) k_I + F_{22}(\alpha) k_{II},
 \tag{19}$$

where  $k_I$  and  $k_{II}$  are the stress intensity factors at the original crack tip, and  $K_I$  and  $K_{II}$  are those at the extended crack tip, respectively.  $F_{pq}$  ( $p, q=1,2$ ) which are functions of the kink angle  $\alpha$ , are given by

$$F_{11}(\alpha) = 1 - \frac{3}{8} \alpha^2 + \left( \frac{1}{\pi^2} - \frac{5}{128} \right) \alpha^4 + \left( \frac{1}{9\pi^4} - \frac{11}{72\pi^2} + \frac{119}{15360} \right) \alpha^6 + O(\alpha^8),
 \tag{20}$$

$$F_{12}(\alpha) = -\frac{3}{2} \alpha + \left( \frac{10}{3\pi^2} + \frac{1}{16} \right) \alpha^3 + \left( -\frac{2}{\pi^4} - \frac{133}{180\pi^2} + \frac{59}{1280} \right) \alpha^5 + O(\alpha^7),
 \tag{21}$$

$$F_{21}(\alpha) = \frac{1}{2} \alpha - \left( \frac{4}{3\pi^2} + \frac{1}{48} \right) \alpha^3 + \left( -\frac{2}{3\pi^4} + \frac{13}{30\pi^2} - \frac{59}{3840} \right) \alpha^5 + O(\alpha^7),
 \tag{22}$$

$$F_{22}(\alpha) = 1 - \left( \frac{4}{\pi^2} + \frac{3}{8} \right) \alpha^2 + \left( \frac{8}{3\pi^4} + \frac{29}{18\pi^2} - \frac{5}{128} \right) \alpha^4 + \left( -\frac{32}{15\pi^6} - \frac{4}{9\pi^4} - \frac{1159}{7200\pi^2} + \frac{119}{15360} \right) \alpha^6 + O(\alpha^8).
 \tag{23}$$

Using these equations, the energy release rate along the kink can be calculated by

$$G = \frac{\kappa + 1}{8\mu} (K_I^2 + K_{II}^2),
 \tag{24}$$

in which  $\kappa$  is a function of Poisson's ratio and  $\mu$  is the shear modulus.

The crack path criterion based on the stress distribution prior to crack extension was proposed by Erdogan and Sih [11], where they assumed that a crack would propagate in the direction normal to the maximum hoop stress. By differentiating



Eq. (17) with respect to  $\theta$ , we can obtain the equation which gives rise to the direction as

$$k_I \sin \alpha + k_{II} (3 \cos \alpha - 1) = 0, \tag{25}$$

Another criterion is the geometry-based one, the so-called local symmetry criterion proposed by Banichuk [1] and Goldstein and Salganik [2, 3], where they assume that the crack extends under pure Mode-I condition along the crack extension, i.e.

$$K_{II}(\alpha) = F_{21}(\alpha)k_I + F_{22}(\alpha)k_{II} = 0. \tag{26}$$

In contrast to the condition (25), the stress intensity factor after crack extension is required for the crack path prediction. Sometimes the explicit simplicity of the criterion (25) is in favor over the criterion (26), which may be consistent but numerically implicit. In order to examine whether the above two criteria are equivalent to each other or not, we calculate determinant,  $D_1$  of Eqs. (25) and (26) with respect to  $k_I$  and  $k_{II}$ ,

$$\begin{aligned} D_1 &= \sin \alpha F_{22}(\alpha) - (3 \cos \alpha - 1) F_{21}(\alpha) \\ &= -\left(\frac{4}{3\pi^2} - \frac{1}{4}\right)\alpha^3 + \left(\frac{4}{\pi^4} - \frac{53}{90\pi^2} - \frac{1}{32}\right)\alpha^5 + O(\alpha^7), \end{aligned} \tag{27}$$

where  $F_{2q}$  ( $q=1,2$ ) are expanded in terms of  $\alpha$ . The result does not vanish so that these two criteria are independent with each other, and the difference appears in the third order term with respect to  $\alpha$ . A more fundamental question raised from this result is that since the crack path predicted by the maximum hoop-stress criterion certainly induces a finite Mode-II stress intensity factor at the crack tip after an infinitesimally small crack extension, we cannot expect a smooth trajectory of a crack path i.e., an infinitesimally small zig-zag crack path along the kink.

The energy-based criterion is the one which maximizes the energy release rate so that the potential energy of the elastic body is minimized, Wu [9]. Using the energy release rate calculated by Eq. (24), this condition is attained by

$$\frac{dG}{d\alpha} = \frac{\kappa + 1}{4\mu} \left( K_I \frac{dK_I}{d\alpha} + K_{II} \frac{dK_{II}}{d\alpha} \right) = 0, \tag{28}$$

and

$$\frac{d^2G}{d\alpha^2} < 0. \tag{29}$$

Suppose that the equivalence of the criteria (26) and (28) holds, then the second term of the right-hand side of Eq. (28) vanishes so that

$$K_I \frac{dK_I}{d\alpha} = 0. \tag{30}$$

Since  $K_I$  can naturally be assumed to be positive during the fracturing process, we must have the stationary condition of  $K_I$ , i.e.,

$$\frac{dK_I}{d\alpha} = F'_{11}(\alpha)k_I + F'_{12}(\alpha)k_{II} = 0, \tag{31}$$

in which prime denotes the differentiation with respect to  $\alpha$ , and  $F'_{1q}(\alpha)$  ( $q=1,2$ ) are given by

$$F'_{11}(\alpha) = -\frac{3}{4}\alpha + \left(\frac{4}{\pi^2} - \frac{5}{32}\right)\alpha^3 + \left(\frac{2}{3\pi^4} - \frac{11}{12\pi^2} + \frac{119}{2560}\right)\alpha^5 + O(\alpha^7), \tag{32}$$



$$F'_{12}(\alpha) = -\frac{3}{2} + \left(\frac{10}{\pi^2} + \frac{3}{16}\right)\alpha^2 + \left(-\frac{10}{\pi^4} - \frac{133}{36\pi^2} + \frac{59}{256}\right)\alpha^4 + O(\alpha^6). \quad (33)$$

In order to examine the similarity of the criteria given by Eqs. (31) and (26), we again calculate the determinant  $D_2$  of the coefficients of  $k_I$  and  $k_{II}$ , which is given by

$$D_2 = F_{21}(\alpha) F'_{12}(\alpha) - F'_{11}(\alpha) F_{21}(\alpha) = \frac{2}{45\pi^2}\alpha^5 + O(\alpha^7). \quad (34)$$

It is interesting to note that these two criteria are identical up to the 4th order with respect to the kink angle  $\alpha$ . Also, from the above discussions, the direction which maximizes the Mode-I stress intensity factor is another distinct criterion. In Fig. 3, one may compare the difference or similarity of kink angles predicted by these criteria. It is rather difficult to numerically distinguish the difference of the local symmetry and maximum energy release rate criteria. We shall discuss the local symmetry criterion in the following discussions, because it may lead to slightly kinked and curved crack propagation in a relatively simple way by using the perturbation solution.

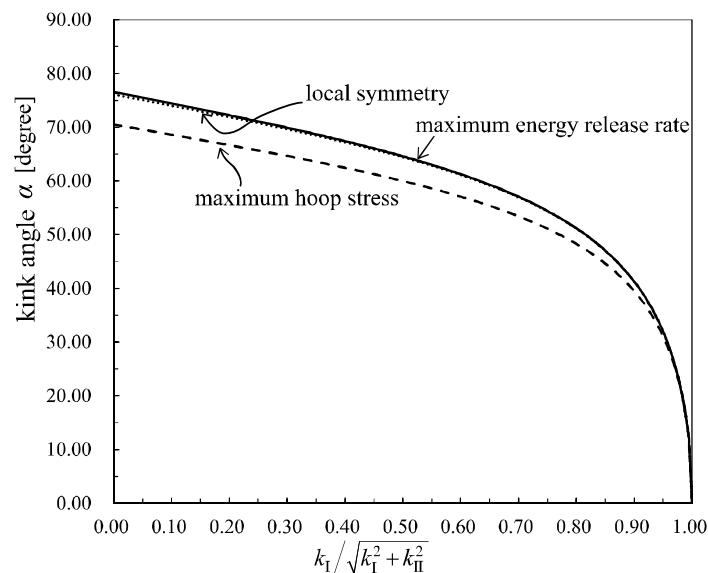


Figure 3: Comparison of the kink angles under mixed mode conditions [16].

## CRACK PATH PREDICTION AND ITS STABILITY

### *Crack Path Prediction Based on the Local Symmetry Criterion*

Since a smooth path can be obtained by the local symmetry criterion and the equivalence of the maximum energy release rate may be expected within a small kink angle, discussions are made based on this criterion. We shall consider the prediction of a kinked and curved crack path based on the first order perturbation solution (15) and (16) at an arbitrarily extended crack tip from a straight crack, so that the crack path is obtained by substituting Eq. (16) into the local symmetry criterion (26), and the shape parameters of the crack path are obtained as [6-8]

$$\alpha = -2 \frac{k_{II}}{k_I}, \quad (35)$$

$$\beta = \frac{8}{3} \sqrt{\frac{2}{\pi}} \frac{T}{k_I} \alpha, \quad (36)$$



$$\gamma = -\left(\overline{k_{21}k_{I1}} + \overline{k_{22}k_{II1}} + \frac{b_{II}}{2}\right) \frac{1}{k_{I1}} + \left[ \left\{ (2\overline{k_{22}} - \overline{k_{11}})k_{I1} + \frac{1}{2}b_{I1} \right\} \frac{1}{2k_{I1}} + 4(T/k_{I1})^2 \right] \alpha. \quad (37)$$

*Crack Path Stability*

Based on the shape parameters obtained by the crack path prediction, crack path stability in a symmetric homogeneous brittle solid is considered, Leever *et al.* [13], Broberg [14], Pook [15]. We shall investigate the cases where the geometry of the body is symmetric with respect to the initial straight crack line, and where the presence of a small asymmetric loading or slight material inhomogeneity which may produce a small Mode-II stress-intensity factor  $k_{II}$  at the original crack tip, leads to non-collinear crack growth with small, initial kink angle  $\alpha$ . The crack path stability is then examined by taking into account the second and third terms of Eq. (1).

Let the crack growth profile be normalized by a representative length,  $L_s$ , of the body. We set

$$\lambda^* = \alpha \left( \frac{b}{L_s} \right) \left[ 1 + \left( \frac{\beta^*}{\alpha} \right) \sqrt{\frac{b}{L_s}} + \left( \frac{\gamma^*}{\alpha} \right) \left( \frac{b}{L_s} \right) \right], \quad (38)$$

where

$$\lambda^* = \frac{\lambda}{L_s}, \quad \beta^* = \beta \sqrt{L_s}, \quad \text{and} \quad \gamma^* = \gamma L_s. \quad (39)$$

The crack path stability is determined by the quantity  $D_s$ , given by

$$D_s = \left( \frac{\beta^*}{\alpha} \right) + \left( \frac{\gamma^*}{\alpha} \right) \sqrt{\frac{b}{L_s}} \begin{cases} < 0 : \text{stable} \\ > 0 : \text{unstable} \end{cases}, \quad (40)$$

where

$$\beta^* / \alpha = \frac{8}{3} \sqrt{\frac{2}{\pi}} \frac{T}{k_{I1}} \sqrt{L_s}, \quad (41)$$

and

$$\gamma^* / \alpha = \left[ \left( \overline{k_{21}k_{I1}} + \overline{k_{22}k_{II1}} + \frac{b_{II}}{2} \right) \frac{1}{2k_{II1}} + \left\{ (2\overline{k_{22}} - \overline{k_{11}})k_{I1} + \frac{1}{2}b_{I1} \right\} \frac{1}{2k_{I1}} + 4(T/k_{I1})^2 \right] L_s. \quad (42)$$

The crack path stability for predominantly Mode-I loading conditions can be determined from the values of  $\beta^*/\alpha$  and  $\gamma^*/\alpha$ . It has been confirmed that if the small imperfection parameter,  $k_{II}$ , is considered to be independent on the crack length, sum of the first three terms in the right hand side of Eq.(42) vanish, so that Eqs. (36) and (42) are expressed only in terms of the quantities which do not depend on the small asymmetric loading condition. If we represent the stability condition (40) in terms of  $\beta^*/\alpha$  and  $\gamma^*/\alpha$ , we have

- (i)  $\beta^* / \alpha < 0$  and  $\gamma^* / \alpha < 0$  : stable
- (ii)  $\beta^* / \alpha > 0$  and  $\gamma^* / \alpha > 0$  : unstable
- (iii)  $\beta^* / \alpha < 0$  and  $\gamma^* / \alpha > 0$  :  $\begin{cases} \text{stable for } 0 < b / L_s < (\beta^* / \gamma^*)^2 \\ \text{unstable for } b / L_s > (\beta^* / \gamma^*)^2 \end{cases}$  (43)
- (iv)  $\beta^* / \alpha > 0$  and  $\gamma^* / \alpha < 0$  :  $\begin{cases} \text{unstable for } 0 < b / L_s < (\beta^* / \gamma^*)^2 \\ \text{stable for } b / L_s > (\beta^* / \gamma^*)^2 \end{cases}$

Stable and unstable paths defined by (43) are illustrated in Fig.4.

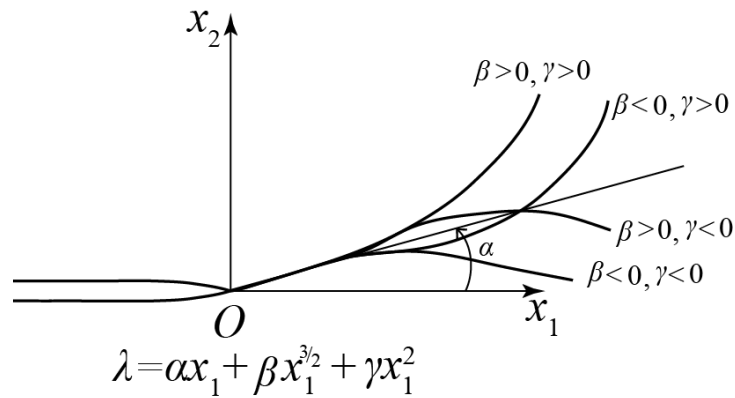


Figure 4: Comparison of the crack path stability [12].

As can be seen from the condition (43), the present concept of crack path stability includes the length parameter  $h/L_s$  and the stability may depend on the range of the crack growth length considered. An initially unstable crack growth path may recover its straight direction with increasing crack length under the condition (iv) in (43). On the other hand, if condition (iii) holds, the crack path may become unstable in the range  $h/L_s > (\beta^*/\gamma^*)^2$ .

The Cotterell and Rice theory [4] is based on the first term of the condition (40), leading to the following criterion for crack path stability:

$$\beta^*/\alpha \begin{cases} < 0 : \text{stable} \\ > 0 : \text{unstable} \end{cases}, \tag{44}$$

which is equivalent to

$$T \begin{cases} < 0 : \text{stable} \\ > 0 : \text{unstable} \end{cases} \tag{45}$$

This may be considered as a *local stability* criterion for the branched and curved crack extension, while the condition (43) may be regarded as an *intermediate range of stability* concept, in which the stability conditions change with increasing crack length. This theoretical prediction is borne out by experimental observations.

A double-cantilever beam specimen is shown in Fig. 5, where the length  $L$  equals  $6B$ . The characteristic length is  $L_s=B$ . The numerical values of  $\beta^*/\alpha$  and  $\gamma^*/\alpha$  are given in Fig. 6, which show the condition

$$\beta^*/\alpha > 0 \quad \text{and} \quad \gamma^*/\alpha > 0, \tag{46}$$

except for an extremely long initial crack. In this case the value of  $D_s$ , given by (40), is always positive, so that an unstable crack path is expected. On the contrary, when the initial crack is extremely long and the crack tip is very close to the right-hand edge of the specimen, we have

$$\beta^*/\alpha > 0 \quad \text{and} \quad \gamma^*/\alpha < 0, \tag{47}$$

where the intermediate range of stability may exist. The experimental results [12, 24], are shown in Fig. 7, where sharp crack curving is observed and the final break-off of the specimen may occur at either the upper or the lower surfaces. However, if the initial straight crack is extremely long and its tip is close to the right-hand edge of the specimen, crack curving is stabilized after some crack extensions as predicted by the theory.

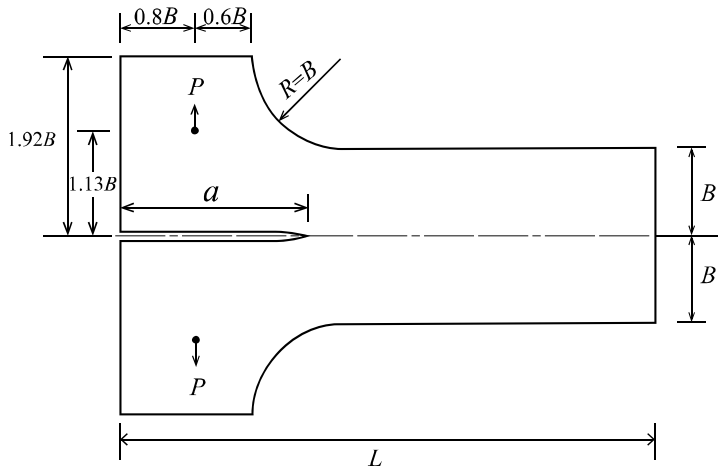


Figure 5: Double-cantilever beam specimen [12, 24].

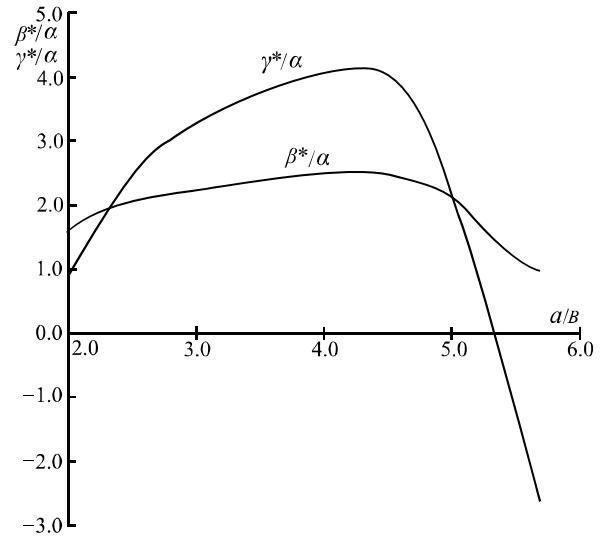


Figure 6: Stability parameters for a double-cantilever beam specimen [12, 24].

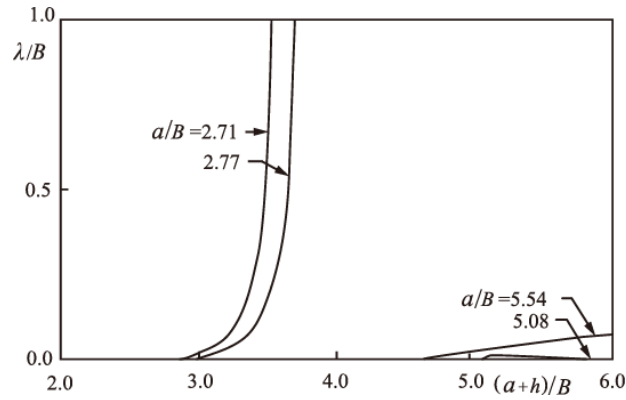


Figure 7: Crack paths observed in double-cantilever beam specimens [12, 24].

### Energy Consideration of Crack Paths for Inhomogeneous Fracture Toughness

Following Bilby and Cardew [20], the elastic energy release rate  $G$  due to the slightly kinked and curved crack extension can be calculated by Eq.(24) for a homogeneous material, where  $K_I$  and  $K_{II}$  are the stress intensity factors at the extended crack tip. Substitution of Eqs. (13) and (14) into Eq. (24) leads to an expansion of  $G$  in an ascending order of  $\sqrt{b}$  [7], and it is given by,

$$G = G_0(\alpha; k_I, k_{II}) + O(\sqrt{b}) \quad (48)$$

where  $G_0$  is obtained as

$$G_0(\alpha; k_I, k_{II}) = \frac{\kappa+1}{8\mu} \left\{ \left( 1 - \frac{\alpha^2}{2} \right) k_I^2 - 2\alpha k_I k_{II} + \left( 1 + \frac{\alpha^2}{2} \right) k_{II}^2 \right\} \quad (49)$$

The first and second variations of  $G_0$  with respect to  $\alpha$  are calculated as

$$\delta_\alpha G_0 = -\frac{\kappa+1}{8\mu} \left\{ (k_I^2 - k_{II}^2) \alpha + 2k_I k_{II} \right\} \delta\alpha \quad (50)$$



$$\delta_{\alpha}^2 G_0 = -\frac{\kappa+1}{8\mu} (k_I^2 - k_{II}^2) \delta\alpha^2 \quad (51)$$

As far as the condition  $k_I \gg |k_{II}|$  holds, conditions (50) and (51) indicate that the kink angle  $\alpha$  is given by

$$\alpha = -\frac{2k_I k_{II}}{k_I^2 - k_{II}^2} = -\frac{2k_{II}}{k_I} + O\left\{\left(-\frac{2k_{II}}{k_I}\right)^3\right\} \quad (52)$$

which gives rise to the maximum elastic energy release rate of the body. This result together with Eq. (35) in the previous section may designate equivalent crack paths by employing the conditions of local symmetry and maximum energy release rate in homogeneous materials within the second order approximation theory.

Considering material inhomogeneity such as a local degradation zone, a crack may be kinked and curved due to the spatial variation of the fracture toughness. The method presented here may be effective to obtain possible crack paths in materials with inhomogeneous fracture toughness. Let us consider a crack under pure Mode-I loading condition, whose tip intersects a line degradation zone oriented at angle  $\alpha^*$  (see Fig. 8), where the critical energy release rates for the base material and the degraded material are  $G_c$  and  $G_c^*$ , respectively. If the crack extends in the base material, Eq. (52) is applicable, which obviously leads to the straight crack extension. The stress intensity factor at the instance of fracture is calculated from Eq. (49) and given by

$$k_I = \sqrt{\frac{8\mu G_c}{\kappa+1}} \quad (53)$$

In contrast, if the crack extends in the degraded zone, the kink angle is  $\alpha^*$ , and the corresponding stress intensity factor at the instance of kinked propagation is also calculated by Eq. (49) as

$$k_I^* = \sqrt{\frac{8\mu G_c^*}{(\kappa+1)\left(1-\frac{\alpha^{*2}}{2}\right)}} \quad (54)$$

The crack may actually extend in the degraded zone under the condition  $k_I^* < k_I$ . Substitution of Eqs. (53) and (54) into this inequality leads to the following relationship between the angle of inclination and the material properties;

$$G_c^* < \left(1-\frac{\alpha^{*2}}{2}\right) G_c \quad (55)$$

which cannot be predicted by a conventional stress criterion. When one applies the inequality (55), the resulting inclination angle  $\alpha^*$  should be less than 30–40°, where the second order perturbation solution of the stress intensity factors is practically applicable.

## BRITTLE FRACTURE ALONG BUTT-WELD

### *Morphological Aspects of Brittle Fracture along Butt-Weld*

One of the most hazardous failure modes of welded steel structures is an instantaneous fracture due to crack propagation along weldment, which may lead to the catastrophic failure of the total structure. Typical crack paths along a welded joint are schematically illustrated in Fig. 9, where the applied stress  $\sigma_a$  and the welding residual stress  $\sigma_r$  acting parallel to the weldment are also sketched, Hall *et al.* [25], Munse [26], Wells [27].

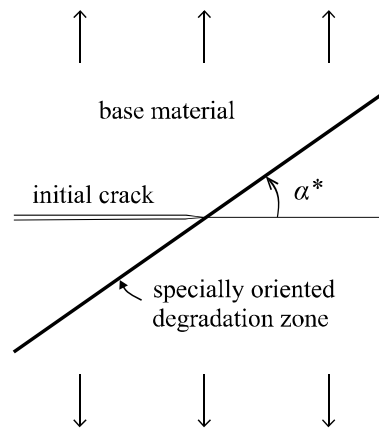


Figure 8: A Mode-I crack intersecting a line-degradation at angle  $\alpha^*$ .

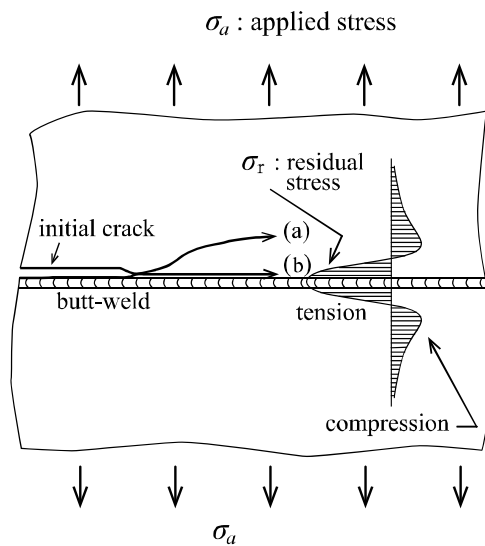


Figure 9: A brittle crack propagating parallel to a welded joint; (a) crack propagation in the base metal; (b) crack propagation along butt-weld joint.

Early experimental results of the ESSO tests, which were performed by Kihara *et al.* [28, 29] using welded mild steel plates, indicate that a brittle crack initiated along the welded joint turns off the welding line and propagates into the base metal as illustrated by the crack path (a) in Fig.9. A brittle crack propagates in a region a finite distance away from the welding line, where the distance increases with decreasing the ratio of applied and residual stresses. These morphological characteristics of brittle fracture of welded mild steel plates had been confirmed later by more sophisticated dynamic crack propagation and crack arrest tests using middle and large size specimens, SR147 [30] and SR153 [31]. In the case of welded mild steel plates, since cracks are expected to turn off the welding line due to the high tensile welding residual stress acting parallel to the welding line [32], the localized decrease of fracture toughness in the heat-affected zone does not play an important role in relation to the crack arrest capability of a welded total structure.

Kihara and Ikeda [33] observed crack paths of welded high tensile steel plates, which exhibited different behavior from what was observed in welded mild steel plates. These morphological aspects of brittle fracture of welded plates, which were made of high tensile steel for ship structural use, were later investigated in detail by the Shipbuilding Research Association of Japan, SR147 [30], and SR153 [31], and SR169 [34]. It is observed in these experiments that although in some cases cracks turn off the welding line and propagate in the base metal, they sometimes propagate along the welding line as is illustrated by the path (b) in Fig. 9.

Since the ratio of applied stress  $\sigma_a$  of high tensile steel plates and the maximum tensile residual stress is relatively high in comparison with that for the mild steel plates, and since the relatively large decrease of the fracture toughness may be expected near the bond zone, these effects could cause the brittle fracture along the butt-weld for high tensile steel plates.



In this case, the conditions corresponding to the crack propagation in the base metal and along butt-weld should be clearly distinguished for the evaluation of the crack arrest capability of welded structures. We shall review some analytical studies in the following subsection.

*Analytical Model for Crack Path Prediction*

Investigations are made for a butt-weld joint under a uniaxial tensile stress  $\sigma_a$  applied normal to the joint [7]. The longitudinal component of welding residual stress  $\sigma_r$  is assumed to be constant in the region under consideration. As shown in Fig. 10, the initial crack of length  $2a$  is assumed to be parallel to the welding line. Material deterioration is observed along the heat-affected zone, which is modeled as a line degradation being also parallel to the welding line at a distance  $L_y$  from the initial crack line. The resistance forces of crack propagation are denoted by  $G_c$  for base and weld metals, and  $G_c^*$  for the degradation zones, respectively. Brittle crack propagation is assumed to occur from the right-hand side of the crack tip, at which we choose the origin of the Cartesian coordinate system  $O-x_1x_2$ . Since a slightly kinked and curved crack extension may be expected, the crack intersects the degradation line at an angle  $\alpha^*$  with  $x_1 = b^*$ .

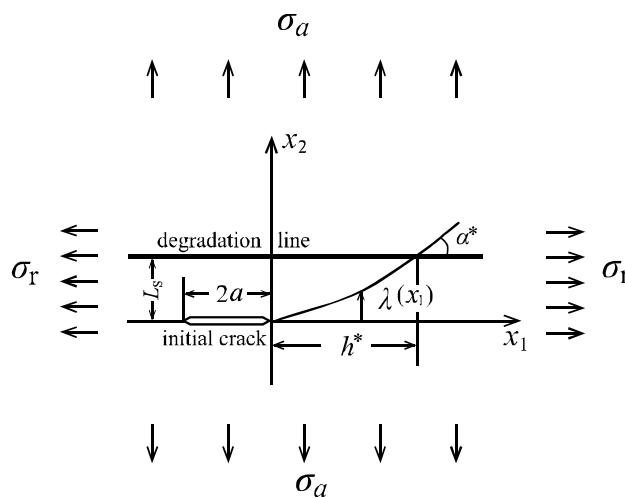


Figure 10: A mathematical modeling of curved crack propagation along butt-weld.

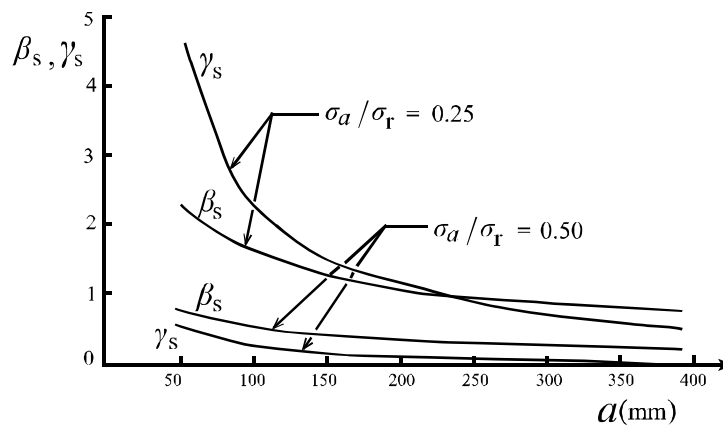


Figure 11: Crack path destabilizing factors  $\beta_s = \beta^* / \alpha$  and  $\gamma_s = \gamma^* / \alpha$  [7, 16].

As far as the initial crack tip is embedded in a homogeneous material, a crack path can be determined by the local symmetry criterion by Eqs.(35)-(37), using the stress field parameters such as  $k_{I1}$ ,  $k_{II1}$  and *etc.* at the original crack tip. This will simply lead to  $\alpha = \beta = \gamma = 0$  under the pure Mode-I condition, but this straight crack extension could occur only for the perfect system, which means that the loading condition and the geometry have the perfect symmetry with respect to the crack line. We consider that non-collinear crack propagation is caused by some load-induced or material-induced



disturbances in the system with a small initial kink angle  $\alpha$  at the original crack tip, which can be interpreted as the initial imperfection of the system. The crack path stability is then examined by taking into account the second and third terms of Eq. (1). The crack path stability is determined by the condition (40). Fig. 11 shows the crack path destabilizing factors,  $\beta_s = \beta^* / \alpha$  and  $\gamma_s = \gamma^* / \alpha$ , for the present case, where the ratios of applied stress and maximum residual stress are chosen as 0.25 and 0.5. In the case where the applied stress level is relatively low, these parameters have high values, so that crack paths of low stress brittle fracture initiated from a small initial crack may be curved to the base metal. As the crack further extends, it begins to intersect the line degradation zone. At this point the question arises as to whether the crack intersects the zone and penetrates into the base metal, or it kinks to the degradation zone. In order to answer this question, we calculate the angle  $\alpha^*$  formed by the crack and the degradation line, which will lead to condition of kinked crack extension along the degradation line by the inequality (55).

### *Effect of Residual Stress and Toughness along Butt-Weld*

Case-studies are shown for the initial half crack length  $a = 100, 200, 300, 400, 500$  mm. Since the distance,  $L_s$  between the initial crack line and the degradation line is of the order of the bead-width, it is selected as 50 mm. The imperfection parameter is selected as  $\alpha = 2.5^\circ$ . Based on the theory presented in the previous subsection, we can determine the critical curves which distinguish the crack propagation in the base metal and in the degraded zone, respectively. Such curves are illustrated in Fig. 12, in which if the ratio of the applied stress and the residual stress,  $\sigma_a / \sigma_r$ , and the ratio of the toughness of degraded zone and the base metal,  $G_c^* / G_c$  fall into the lower right-hand side of the respective curves, a brittle crack may propagate along the degradation zone. It can be quantitatively understood that if the tensile residual stress acting parallel to the welded joint is relatively low, and if the decrease of fracture toughness in the degraded zone is relatively large, cracks may propagate along the degradation zone. This result qualitatively explains the difference of brittle fracture behavior observed in welded mild steel plates and high tensile steel plates. As observed in Fig. 12, brittle fracture initiating from a longer straight crack has a tendency to propagate along the degradation zone. This means that once a brittle crack has begun to propagate along a welded joint, it is hard to turn it into the base metal.

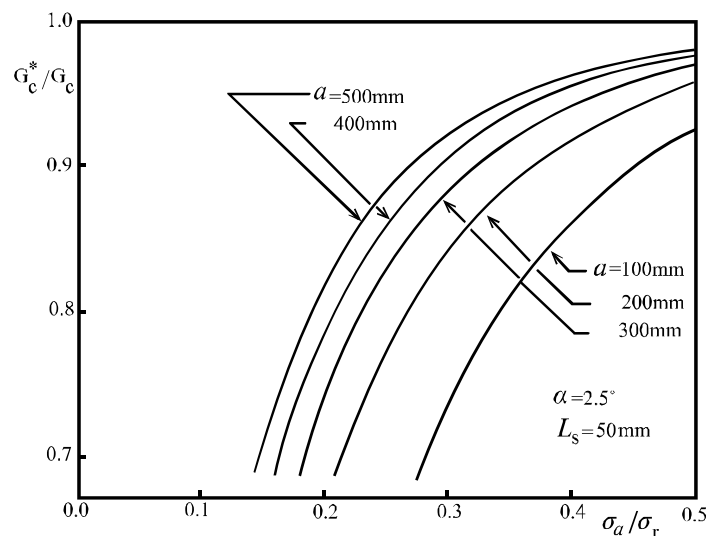


Figure 12: Critical relations between the material degradation and the applied stress; cracks penetrate into the base metal for the conditions corresponding to the upper left regions with respect to the curves [7, 16].

## **FRACTURE CONTROL OF BUTT-WELD OF LARGE CONTAINER SHIPS**

**W**ith the rapid increase of the size of container ships, fracture control of extremely thick plates employed in the deck structure of large container ships has been studied in a project organized by Japan Ship Technology Research Association (JSTRA) [17], which includes the crack arrest design of a brittle crack having unexpectedly started and propagating in the deck structure. Possible scenarios to ensure the crack arrest performance in the hatch-side coaming and upper deck plates have been proposed by ClassNK [35] focusing attention on the practical

arrest design. As mentioned, brittle cracks propagating along the welded joint deviate their paths from the weld, and penetrate into the base plate possibly due to the effect of welding residual stress. The arrest toughness,  $K_{ar}$ , of a brittle crack in order to prevent the propagation of long brittle cracks was found to be within the range 4,000–6,000 N/mm<sup>3/2</sup> at the service temperature, SR147 [30], which were based on the tests of the steel plates with the thickness less than 35mm used for ship structures. Since the thickness of the plates used for extremely large container ships is 50-80mm, investigations have been made by Yamaguchi *et al.* [36]. For the brittle crack arrest design, certain brittle crack arrest toughness,  $K_{ar}$ , must be ensured for a steel plate used for the arrester, so that an efficient test method has been developed to evaluate brittle crack arrest toughness of extremely thick steel plates. The objective of the arrest design of a brittle crack is to arrest brittle crack propagation at specific locations so that a catastrophic failure of the hull structure is prevented in the event of an unexpected crack initiation. For this purpose, the following functional requirements are introduced;

1. brittle crack should be arrested at specific locations (see Fig. 13),
2. hull girder stress after the arrest should be less than the specified yield stress of the applied steel plates,
3. consequently, a brittle crack initiation does not result in large-scale failure of the hull structure.

In order to achieve these functional requirements, the following two methods of crack arrest are introduced;

*Material arrest:* to arrange materials of high resistance to brittle crack propagation to arrest brittle cracks, and

*Structural arrest:* to discontinue crack propagation paths by appropriate structural arrangements.

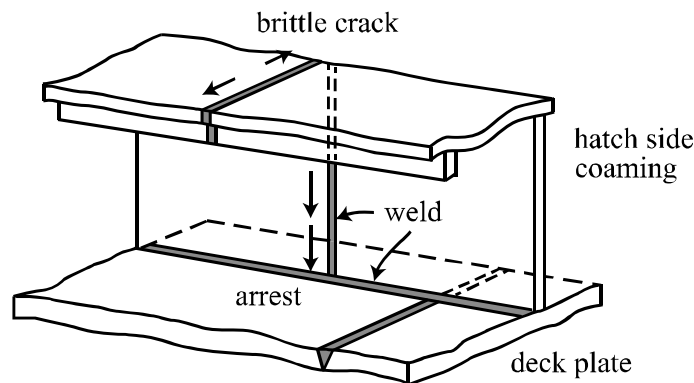


Figure 13: An example of brittle crack arrest in a deck structure.

Based on the large-scale crack arrest tests for the determination of minimum brittle crack arrest toughness, it has been found that the toughness  $K_{ar} = 6,000$  N/mm<sup>3/2</sup> may be an upper limit for crack propagation in the ultra-wide duplex ESSO tests which can evaluate  $K_{ar}$  without considering structural discontinuity, Inoue *et al.* [37]. In order to ensure the crack arrest in the deck plate made of high-arrest steel plate, a minimum shift of butt-weld as illustrated in Fig. 13 has also been recommended.

## CONCLUSIONS

**P**erturbation analyses of a kinked and curved crack have been reviewed in the present paper focusing attention on the crack path criteria and crack path stability induced by local stress biaxiality or by inhomogeneous fracture toughness. Having reviewed experimental and theoretical studies of brittle crack propagation paths along butt-weld, the concept of fracture control of extremely thick plates of high tensile steel, which are applied to the deck structures of recently developed large container ships, are presented.

## REFERENCES

- [1] Banichuk, N.V., Determination of the form of a curvilinear crack by small parameter technique. *Mekhanika Tverdogo Tela*, 7-2 (1970) 130–137. (in Russian)
- [2] Goldstein, R.V., Salganik, R.L., Plane problem of curvilinear cracks in an elastic solid. *Mekhanika Tverdogo Tela*, 7-3



- (1970) 69–82. (in Russian)
- [3] Goldstein, R.V., Salganik, R.L., Brittle fracture of solids with arbitrary cracks, *Int J Fract*, 10 (1974) 507–523.
- [4] Cotterell, B., Rice, J.R., Slightly curved or kinked cracks, *Int J Fract*, 16 (1980) 155–169.
- [5] Sumi, Y., Nemat-Nasser, S., Keer, L.M., On crack branching and curving in a finite body, *Int J Fract*, 21 (1983) 67–79; Erratum, *Int J Fract*, 24 (1984) 159.
- [6] Sumi, Y., A note on the first order perturbation solution of a straight crack with slightly branched and curved extension under a general geometric and loading condition, *Eng Fract Mech*, 24 (1986) 479–481.
- [7] Sumi, Y., A second order perturbation solution of a non-collinear crack and its application to crack path prediction of brittle fracture in weldment, *Naval Architect Ocean Eng*, 28 (1990) 143–156.
- [8] Karihaloo, B.L., Keer, L.M., Nemat-Nasser, S., Oranratnachai, A., Approximate description of crack kinking and curving, *J Appl Mech*, 48 (1981) 515–519.
- [9] Wu, C.H., Fracture under combined loads by maximum-energy-release-rate criterion, *J Appl Mech* 45 (1978) 553–558.
- [10] Amestoy, M., Leblond, J.B., Crack paths in plane situations-II. Detailed form of the expansion of the stress intensity factors. *Int J Solids Struct*, 29 (1992) 465–501.
- [11] Erdogan, F., Sih, G.C., On crack extension in plates under plane loading and transverse shear, *J Basic Eng*, 85 (1963) 519–527.
- [12] Sumi, Y., Nemat-Nasser, S., Keer, L.M., On crack path stability in a finite body, *Eng Fract Mech*, 22 (1985) 759–771.
- [13] Leevers, P.S., Radon, J.C., Culver, L.E., Fracture trajectories in a biaxially stressed plate, *J Mech Phys Solids*, 24 (1976) 381–395.
- [14] Broberg, K.B., On crack paths, *Eng Fract Mech*, 28 (1987) 663–679.
- [15] Pook, L.P., *Crack Paths*, WIT Press, Southampton, (2002).
- [16] Sumi, Y., *Mathematical and Computational Analyses of Cracking Formation*, Springer, Tokyo, (2014).
- [17] Sumi, Y., *et al.*, Fracture control of extremely thick welded steel plates applied to the deck structure of large container ships, *J Mar Sci Tech*, 18 (2013) 497–514.
- [18] Muskhelishvili, N.I., Some basic problems of the mathematical theory of elasticity, English ed. translated from the 3rd Russian ed., Noordhoff, Groningen-Holland, (1953).
- [19] Bueckner, H.F., A novel principle for the computation of stress intensity factors, *ZAMM*, 59 (1970) 529–546.
- [20] Bilby, B.A., Cardew, G.E., The crack with a kinked tip, *Int J Fract*, 11 (1975) 708–712.
- [21] Bilby, B.A., Cardew, G.E., Howard, I.C., Stress intensity factors at the tips of kinked and forked cracks in: Taplin DMR (Ed.), *Fracture 1977*, vol 3. Pergamon Press, Oxford, (1978) 197–200.
- [22] Hayashi, K., Nemat-Nasser, S., Energy release rate and crack kinking, *Int J Solids Struct*, 17 (1981) 107–114.
- [23] Leblond, J.B., Crack paths in plane situations-I, General form of the expansion of the stress intensity factors, *Int J Solids Struct*, 25 (1989) 1311–1325.
- [24] Sumi, Y., Kagohashi, Y., A fundamental research on the growth pattern of cracks (second report), *J Soc Naval Architects Jpn*, 152 (1983) 397–404. (in Japanese)
- [25] Hall, W.J., Kihara, H., Soete, W., Wells, A.A., Brittle fracture of welded plate. Prentice-Hall, Englewood Cliffs, (1967).
- [26] Munse, W.H., Chapter 8 Brittle fracture in weldments, In: Liebowitz, H. (Ed.), *Fracture: An Advanced Treatise IV Engineering Fracture Design*, Academic Press, New York, (1969) 371–438.
- [27] Wells, A.A., Chapter 7 Effects of residual stress on brittle fracture, In: Liebowitz, H. (Ed.), *Fracture: An Advanced Treatise IV Engineering Fracture Design*, Academic Press, New York, (1969) 337–370.
- [28] Kihara, H., Yoshida, T., Oba, H., Initiation and propagation of brittle fracture in welded steel plate. International Institute of Welding (IIW) Document No. X-217-59 (1959).
- [29] Kihara, H., Masubuchi, K., Effect of residual stress on brittle fracture, *Weld J*, 38 (1959) 159-s.
- [30] Ship Building Research Association of Japan, Report of Research Panel SR147: Strength evaluation of brittle fracture of welded joints of high tensile steel plates with large heat-input in ship hull, <http://www.jstra.jp/html/PDF/SR143-5103.pdf>, (1976). (in Japanese)
- [31] Ship Building Research Association of Japan, Report of Research Panel SR153: Research on brittle fracture and fatigue strength of welded joints of thick steel plates with large heat-input, <http://www.jstra.jp/html/PDF/SR153-5203-1.pdf>, (1977). (in Japanese)
- [32] Sumi, Y., Computational crack path prediction for brittle fracture in welding residual stress fields, *Int J Fract*, 44 (1990) 189–207.
- [33] Kihara, H., Ikeda, K., On brittle fracture initiation (third report)- Brittle fracture initiation characteristics for welded joint of 80 and 60 kgf/mm<sup>2</sup> high strength steels, *J Soc Naval Architects Jpn* 120 (1966) 207–220. (in Japanese)



- [34] Ship Building Research Association of Japan, Report of Research Panel SR169: Research on fracture control of ship structures, <http://www.jstra.jp/html/PDF/SR169-5603.pdf> (1981). (in Japanese)
- [35] Nippon Kaiji Kyokai (ClassNK), Guidelines on Brittle Crack Arrest Design, Tokyo, (2009).
- [36] Yamaguchi, Y., *et al.*, Development of guidelines on brittle crack arrest design - Brittle crack arrest design for large container ships -1 -, In: Proc. 20th ISOPE Conference. Beijing, 4 (2010) 71–79.
- [37] Inoue, T., *et al.*, Required brittle crack arrest toughness  $K_{Ic}$  value with actual scale model tests, In: Proc. 20th ISOPE Conference. Beijing, 4 (2010) 95–101.